Geophysical Techniques Used for Subsurface Exploration of the White River Study Area

Andrew Redifer

Geophysics – Geology G423

December 17, 2013

Abstract

This report describes the data collected by the G423 class in collaboration with the Sedimentary and Stratigraphy class on October 2nd and 3rd, 2013. The purpose of this exercise was to apply geophysical techniques used in exploring the subsurface geology of the field study area located along the east fork of the White River in Lawrence Country, Indiana. The geophysical techniques used were; seismic refraction, electrical resistivity, and ground penetrating radar (GPR). Data collected from geophysical instruments was compared to the core data collected from the sedimentary and stratigraphy class. Results show that he stratigraphy contained alluvium sediments deposited from the White River, glacial till, a mix of alternating sand and silt layers with a gravel layer stratigraphically above the limestone bedrock. The best estimate for depth to bedrock on the floodplain was calculated to be between nine to eleven meters.

Introduction

To fully understand the geology and geological processes that shaped the land a number of approaches needs to be utilized. Topography can be viewed from the naked eye, but to understand the underlying bedrock geologists use geophysical techniques to view the subsurface. Seismic refraction method utilizes the refraction of seismic waves on geologic layers using the different velocities to approximate depth to different strata boundaries. Electrical resistivity is a method that quantifies how strongly a given material opposes the flow of electrical current, and ground-penetrating radar (GPR) is a method that uses radar pulses to image the

subsurface. Using these geophysical techniques allows geologists to image large volumes of the subsurface, and if core data has been conducted the known stratigraphy can be projected throughout the field study area.

The G423 class teamed up with Doug Edmonds and his Sedimentary and Stratigraphy class on October 2nd and 3rd to conduct a field study along the east fork of the White River in Lawrence Country, Indiana ***Figure 1***. The field study area was approximately 600 meters square. Over the course of two days the students were split into six groups; each group was responsible for a different type of data collection. G423 class collected data using the following geophysical methods; seismic refraction, electrical resistivity, and ground penetrating radar (***Figure 2***). Edmonds's class took core samples, observed the geomorphology of the land, and took RTK-GPS points of all flagged locations. The purpose of this trip was to provide students with practice in the field and to familiarize students with tools for collecting geologic data that we could then reduce, and interpret in a creative way that would lead to a deeper understanding of the field study area.

Figure 1. *The above figure is a regional map of the field study site. The red star symbolizes the field study site. (2)*

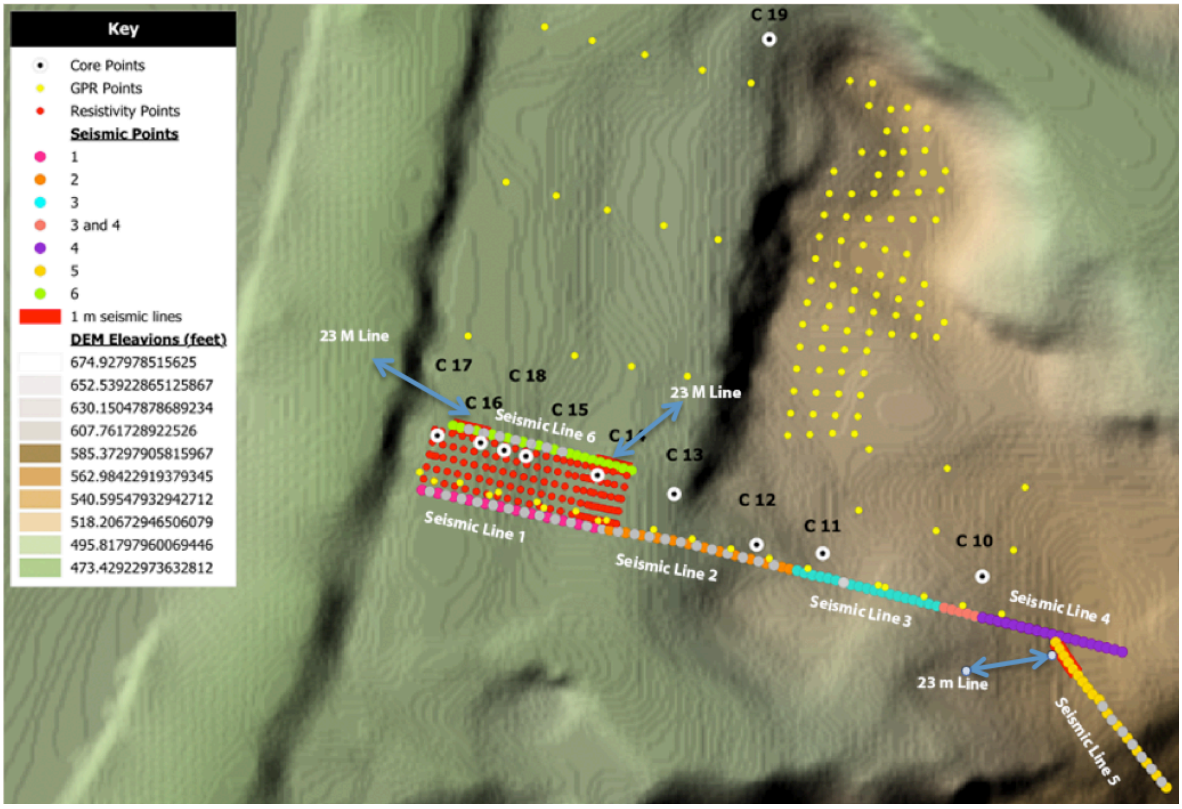

Figure 2. *Overview of the field study area with topography and important GPS positioning of geophysical and core data collected. The above figure was modified from Oliver Wittman's original figure.*

Methods/Theory

As stated above, the two classes were divided into six different data collection groups: seismic refraction, electrical resistivity, ground penetrating radar (GPR), topographic analysis, sediment cores, and geomorphic mapping. Each group had a project leader, however the group as a whole was in charge of collecting their specific data.

The seismic refraction group collected data from six 115-meter lines, and four 23-meter lines (***Figure 2*** & ***Figure 3***). The data collected from the 115-meter lines was used to find bedrock velocities, while the 23-meter lines were used to find soil layer velocities. Members of the seismic refraction team had the job of determining the velocities of geologic units with the end goal of obtaining values for depth to bedrock.

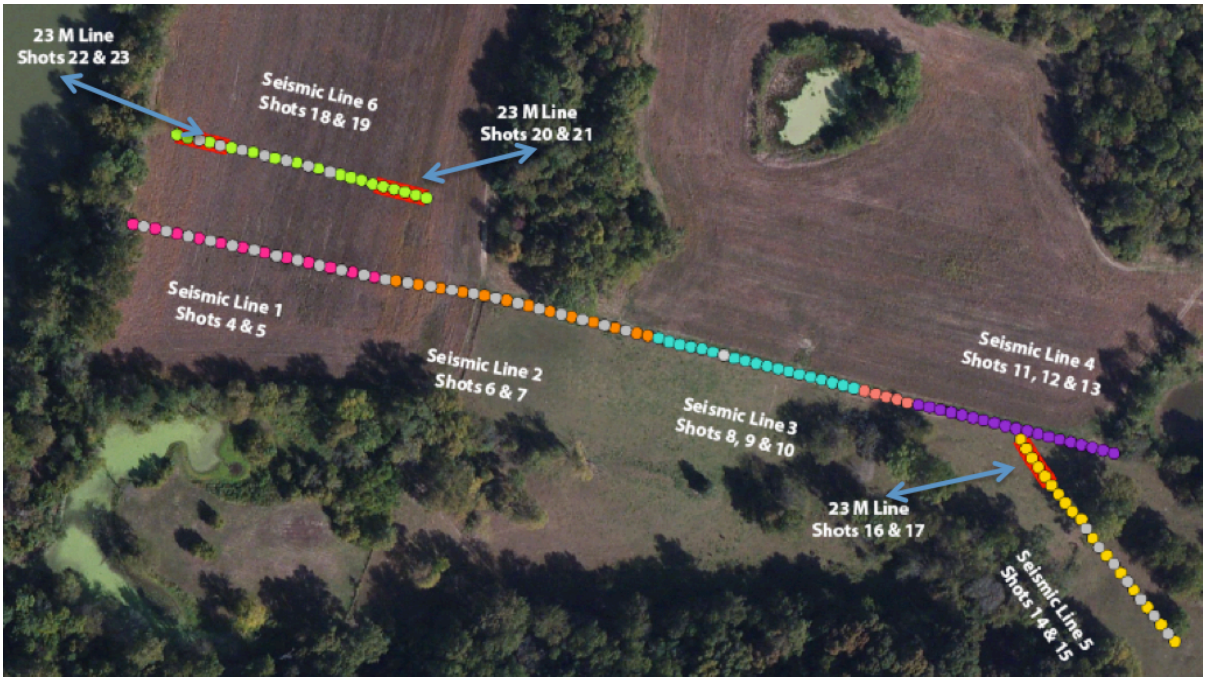

Figure 3. *The figure is an aerial view of the field study area with marked locations of the seismic refraction lines. (Modified from Wittman)*

The seismic refraction method uses an energy source, ours being a sledgehammer hitting a metal plate to produce waves that propagate radially into the subsurface. ***Figure 4*** shows a diagram in which the energy source represents the hammer hitting the plate, and the black arrows show the path of the resulting waves. The type of material that the wave comes into contact with determines how

much of that wave's energy will bypass the layer, and how much of the wave's energy will be refracted back to the surface, arriving at a geophone.

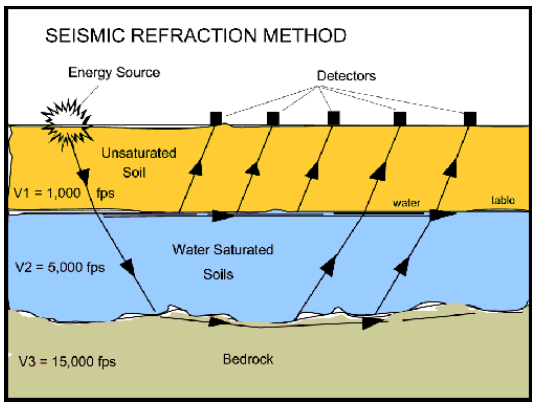

Figure 4. *A simplified diagram of how the seismic refraction method works.* (3)

Figure 4 seen above is a simplified 2-D schematic of this process, but in actuality, the energy from the impact propagates in all directions forming a circular wave front around the energy source. The speed of the produced wave is function of the material it is passing through. Waves travel faster through denser material because on the micro scale objects are more tightly packed and energy can be passed along faster. For example, waves will move more quickly through limestone than unconsolidated sediments

Jason from Advanced Geosciences, Inc. led the electrical resistivity group. The purpose of the electrical resistivity equipment was to measure the relative resistive properties of the subsurface by producing a subsurface resistivity profile to infer changes in stratigraphy and sedimentology. Materials comprised of soil and rocks are essentially nonconductive, except in cases of metallic ores, so the resistivity of soils is primarily governed by the amount of water present. Resistivity

surveys are useful in detecting bodies of anomalous materials, or in estimating the depths of bedrock surfaces. In the case of our study we are interested in estimating the depth to bedrock.

Resistivity is measured in ohmmeters. Ohm's Law is given below in *Equation 1*:

$$V = I * R \qquad \textbf{Equation 1}$$

Resistivity (ρ) is measured in ohmmeters and is given below in *Equation 2*:

$$\rho = R * (\frac{A}{L}) \qquad \textbf{Equation 2}$$

The device used in the field was a SuperSting with Wi-Fi that is a resistivity, induced polarization and self-potential portable instrument. The instrument was connected to a 12 Volt battery and was placed in the center of a cable that had 54 electrodes with two meter spacing between each. The configuration used in our study was a two-dimensional measurement configuration for a dipole-dipole resistivity profile.

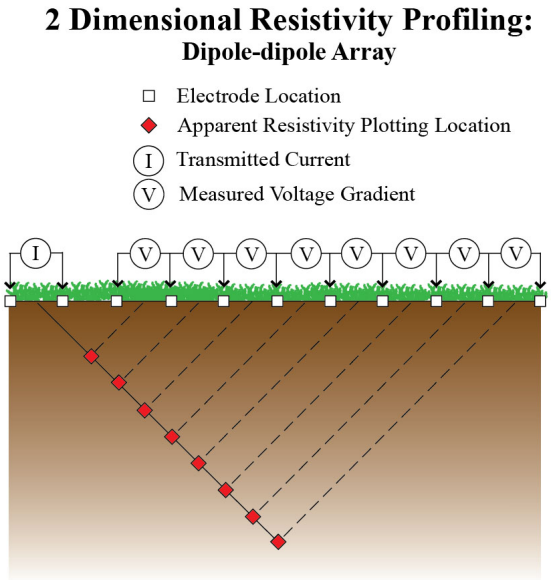

Figure 5. *A simplified diagram of how two dimensional resistivity profiling is arrayed when laid out as Dipole-Dipole. http://www.epa.gov/esd/cmb/GeophysicsWebsite/pages/reference/methods/Surface_Geophysical_Methods/Electrical_Methods/Resistivity_Methods.htm*

Figure 5 above shows a transmitting current dipole (I) followed by a series of potential dipoles (V), which measure the resulting voltage gradient at each station along the line. Measurements are completed by sequentially moving the current down the line. The data collected is displayed as an image that plots the apparent resistivity with depth, which is then contoured using EarthImager 2D, a software developed by Jason's company. Members of the electrical resistivity group collected data from five transects that were all parallel to each other on the flood plain (***Figure 6***).

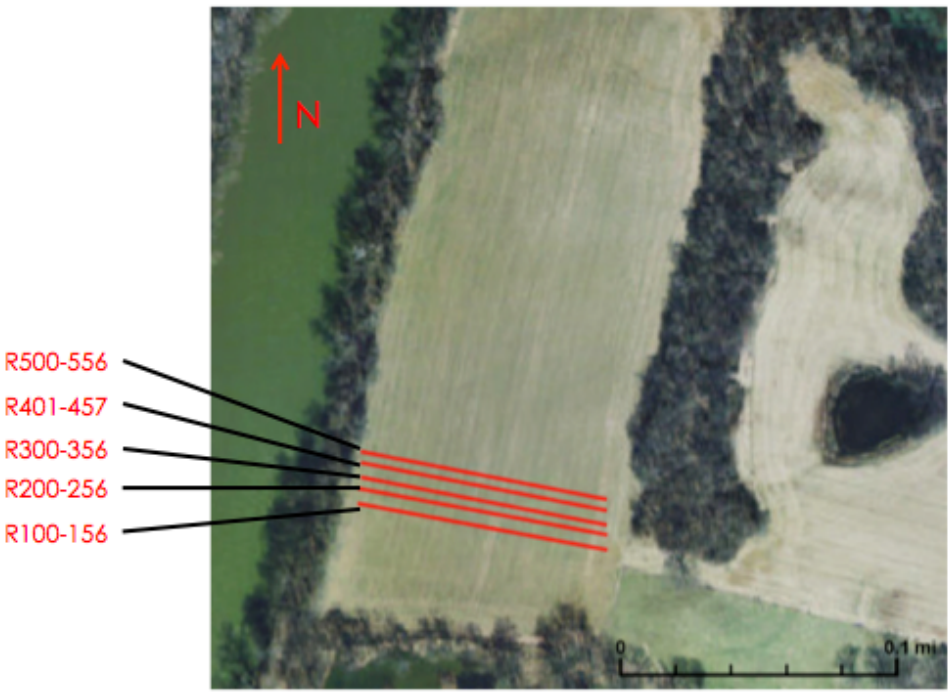

Figure 6. *An aerial view of the approximate locations of the electrical resistivity survey lines. (Fenerty & Baer, 2013)*

The ground penetrating radar (GPR) group used an instrument titled Pulse EKKO-Pro which when installed into a smart cart can be pushed along the surface while transmitting a ground penetrating radar (***Figure 7***). The purpose of this instrument is to determine the thickness and depth of sedimentary layers in the ground's subsurface. The instrument emits high frequency radio signals into the ground that are then detected to build an image, and displays signal time delay and strength. The wave pulses at frequencies ranging from 10 to 100 MHz. Differences in electrical charge in subsurface layers are detected as these wave pulses come in to contact. The major controlling factor is often the water content in the layer. The members of this group took turns collecting data across a thirty one-line grid. The data was converted into a graphical format using the software program, Win EKKO Pro.

Figure 7. *A picture with labels of the GPR instrument and smart kart used to acquire GPR data.*

The topographic analysis group used the Leica RTK (real time kinematic) GPS instrument to collect data (***Figure 8***). This high precision GPS device uses

triangulation to determine its relative position and elevation. Using satellites to communicate with cell phone towers as base stations the relative distance from these stations can be evaluated to the centimeter scale. The topographic group took measurements of two cross sections of the field site, and of locations marked by other groups.

Figure 8. *A picture of the Leica RTK GPS instrument used to collect GPS data. (http://www.geooptic.ru/_image/data/product/1_3200.jpg)*

The sedimentary core group extracted and analyzed nine sediment cores that ranged from sixteen to twenty four feet in length that were one and one quarter in diameter. A Geoprobe Model 54TR rig mounted on the rear of a John Deere 420 tractor extracted the cores (***Figure 9***). The probe used a metal tube that encased a plastic tube to extract the sediment. The metal tube acted as a shield for the inner plastic tube to insure structural integrity during the extraction process. Each core was four feet long, and there were approximately four cores extracted at each location. These sites were extracted incrementally along a path perpendicular from the flow of the river. Members of the sedimentary core team analyzed every ten centimeters of the core to create stratigraphic logs for each site location.

Figure 9. *A picture of the Geoprobe Model 54TR rig mounted on the rear of a John Deere 420 tractor used to extract cores similar to the one used in the study.*

The geomorphic mapping group used their best judgment to determine which land features present on site were important enough to record. Aside from using the observation skills to make qualitative picks was to dig holes and collect samples of important land features. Then by analyzing the sediments they were able to further back up their claims. Cooperating with the topographic analysis group the members were able to determine GPS positions and elevations for land features. The group identified a levee, floodplain, terrace, and marshland in the field area with the help of a digital elevation map (***Figures 10*** & ***11***).

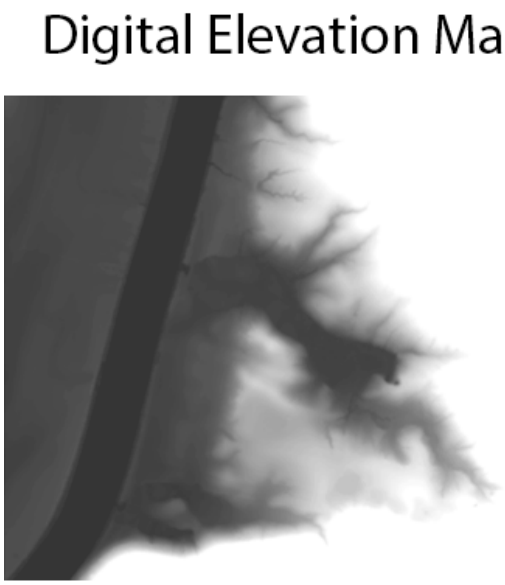

Figure 10. *The above figure is a digital elevation map of the field study area. Lighter colors represent higher elevation. Note the lighter color that rims the river that is the levee. There is also a lighter color in the middle of the floodplain that represents slight rise seen in the central part of the flood plain. (Modified figure from Geomorphology presentation.)*

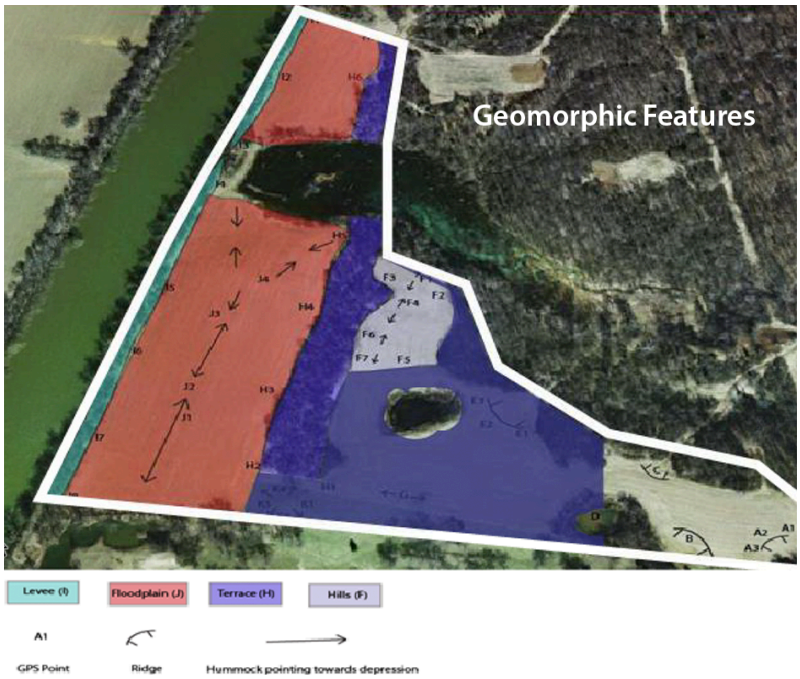

Figure 11. *Assigned geomorphic features for the field study area. Light blue represents the levee, red is the floodplain, and dark blue is the terrace. As for the symbols, A1 represents a GPS point taken for a particular feature, an arrow represents a hummock pointing towards a depression, and the hatched arch represents a ridge. (Modified figure from Geomorphology presentation)*

Data Analysis

a. Seismic refraction:

Snell's Law describes how a travelling wave can be bent while entering a material with a different density (***Figure 12***).

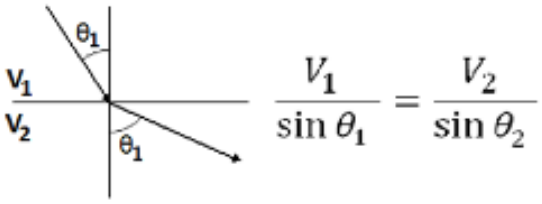

Figure 12. *Snell's Law, where V is the velocity of a wave through a particular solid, and θ is the refraction angle. (4)*

Snell's Law can be used to estimate the travel path of waves through a material. A diagrammatic sketch of such a path is seen below (***Figure 13***).

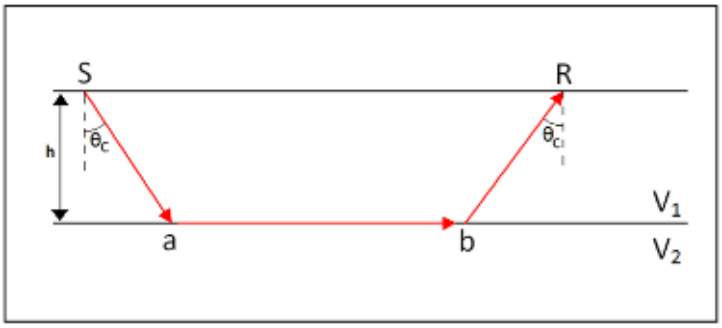

Figure 13*. Simplified diagram of the travel path of a refracted wave from source to receiver. Where 'S' and 'R' stand for the source and receiver, 'V_1' and 'V_2' stand for the wave velocities within different units, 'h' stands for the thickness of the layer, 'θ_c' represents the critical angle, and 'a' through 'b' stands for the distance that the wave travelled along the top of the lower lawyer with velocity V_2. (4)*

The goal of the seismic refraction group was to calculate depth to bedrock. This can be done by knowing the wave's travel time from the energy source to the receiver, the velocities through the two layers, V_1 and V_2, the critical angle, and the distance between the source and receiver.

The experimental data contains the travel times of waves from the source to the receivers at different distances for each seismic line. It is important to note that collected travel times are not for the refracted waves alone, but also includes direct and reflected waves.

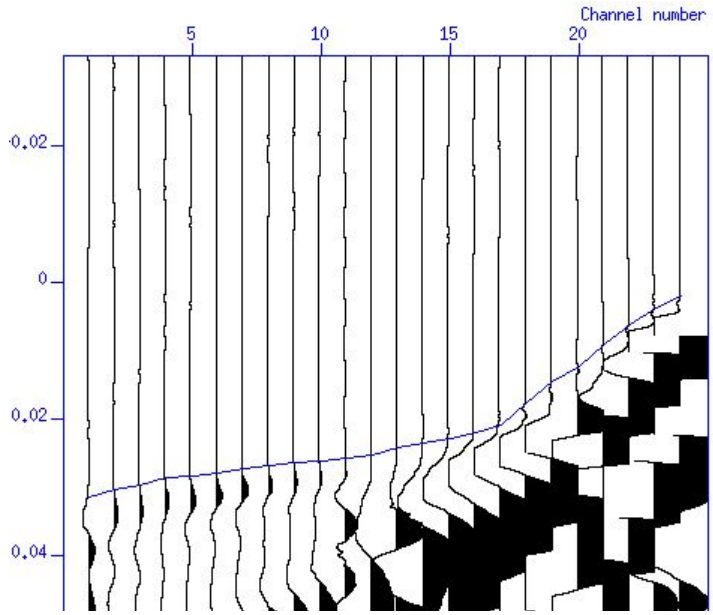

Figure 14. *The above figure is an example of raw experimental data. The x-axis represents the channel number or corresponding geophone that detected the wave. This can easily be changed to represent distance from source. The y-axis is the travel time, or the amount of time taken for the wave to reach the receiver. The blue line drawn in the middle of the figure represents the slope of the first picks. Because the slope is not linear it is indicative of a two-layer problem, or a change in material density. (Davey & Wittman, 2013)*

First break picks were made along each channel number to determine the onset arrivals of refracted signals. The first wave arrivals in ***Figure 14*** show a change in slope at channel 17. These two different slopes represent two different wave types. The steeper slope, closer to the source is the direct wave, and the shallower one is the refracted wave.

In ***Figure 15*** below is a topographic overview of all six 115-meter lines and all three of the 23-meter lines. The 115-meter seismic lines were used to obtain a V_2 where the smaller 23-meter lines were used to obtain velocities for the unconsolidated topsoil or V_1 values. Data reduction for Seismic Line 1 is given below in detail.

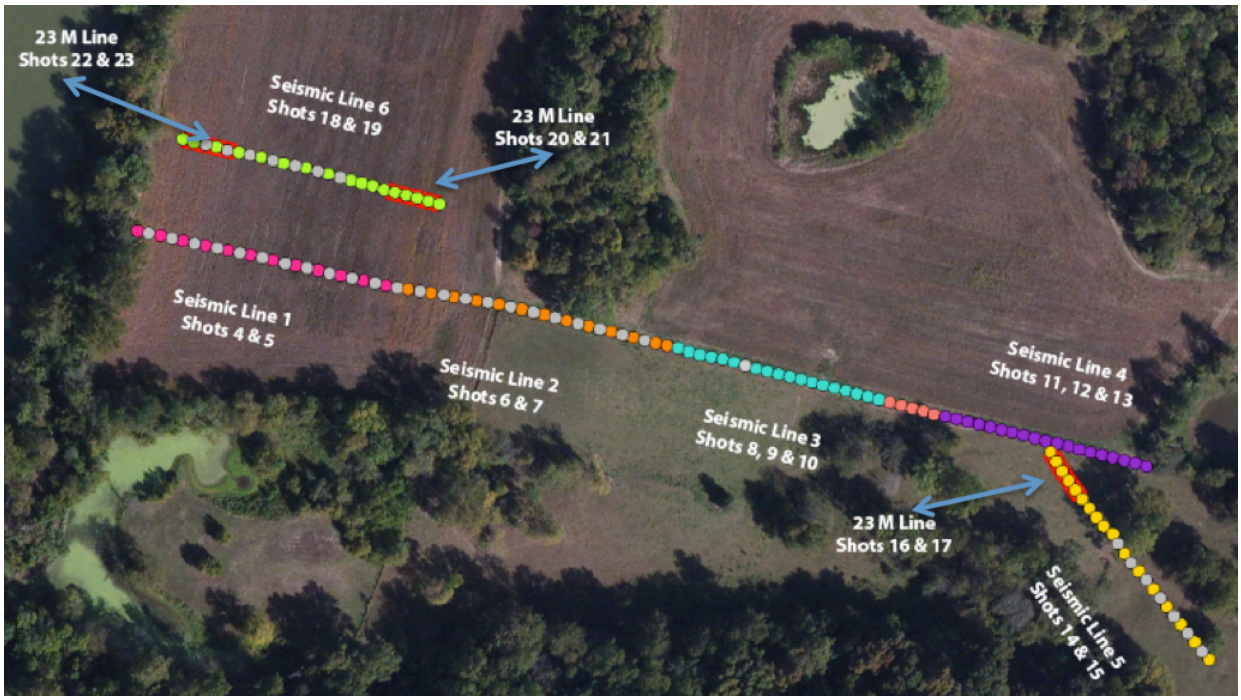

Figure 15. *This figure is a broad aerial view of all surveyed seismic lines. The locations of the geophones represent the dots and their locations and elevations were obtained using the Leica RTK GPS. The figure above shows six 115-meter seismic lines labeled Seismic Line 1-6. Forward and reverse shots were taken at each seismic line and are shown below to correspond to its respective seismic line. The shorter 23-meter seismic lines also have forward and reverse shots and those too are shown below. (Modified from Wittman, 2013)*

Experimental data from two separate shots taken along Seismic Line 1 are shown in ***Figure 16*** below. Shot 4 is the forward time, and shot 5 is the reverse

time. Both times were obtained from first break picks similar to those seen in ***Figure 14*** above.

Shot 4	Channel	Shot 5	Channel
0.0515563	1	0.0059244	1
0.0500284	2	0.016176	2
0.0496464	3	0.0256243	3
0.0475455	4	0.0322937	4
0.0463995	5	0.0324327	5
0.0450625	6	0.0341253	6
0.0427706	7	0.0356562	7
0.0421976	8	0.0392284	8
0.0420067	9	0.0405041	9
0.0410517	10	0.0428005	10
0.0385688	11	0.0448418	11
0.0381868	12	0.0466278	12
0.0393328	13	0.0481588	13
0.0347489	14	0.0512206	14
0.033412	15	0.0530067	15
0.0293195	16	0.0560685	16
0.0277765	17	0.0575995	17
0.0273908	18	0.0598959	18
0.0277765	19	0.0621922	19
0.0266193	20	0.0652541	20
0.0235334	21	0.0688263	21
0.0192902	22	0.0729087	22
0.0158186	23	0.0752582	23
0.0146614	24	0.0791512	24

Figure 16. *This figure shows the travel times and the corresponding channel number (geophone) picked for Shot 4 and Shot 5. Shot 4 is the forward time, and shot 5 is the reverse time.*

For each receiver channel (***Figure 16***) the minus term was computed using *Equation 3*.

$$T_f - T_r \qquad \textbf{Equation 3}$$

Where 'T_f' is time in the forward direction and 'T_r' is time in the reverse direction.

distance (m)	Tf-Tr (s)
115	0.0456319
110	0.0338524
105	0.0240221
100	0.0152518
95	0.0139668
90	0.0109372
85	0.0071144
80	0.0029692
75	0.0015026
70	-0.0017488
65	-0.006273
60	-0.008441
55	-0.008826
50	-0.0164717
45	-0.0195947
40	-0.026749
35	-0.029823
30	-0.0325051
25	-0.0344157
20	-0.0386348
15	-0.0452929
10	-0.0536185
5	-0.0594396
0	-0.0644898

Figure 17*. The above figure is a table that displays the computed minus terms with their corresponding distance in meters.*

The plot below uses the central data seen in ***Figure 17***, where T_f and T_r are both head wave arrivals. Velocity can be obtained by using the slope from ***Figure 18*** below with Equation 4 to solve for V_2.

$$Slope = \frac{2}{V_2} \qquad \text{Equation 4}$$

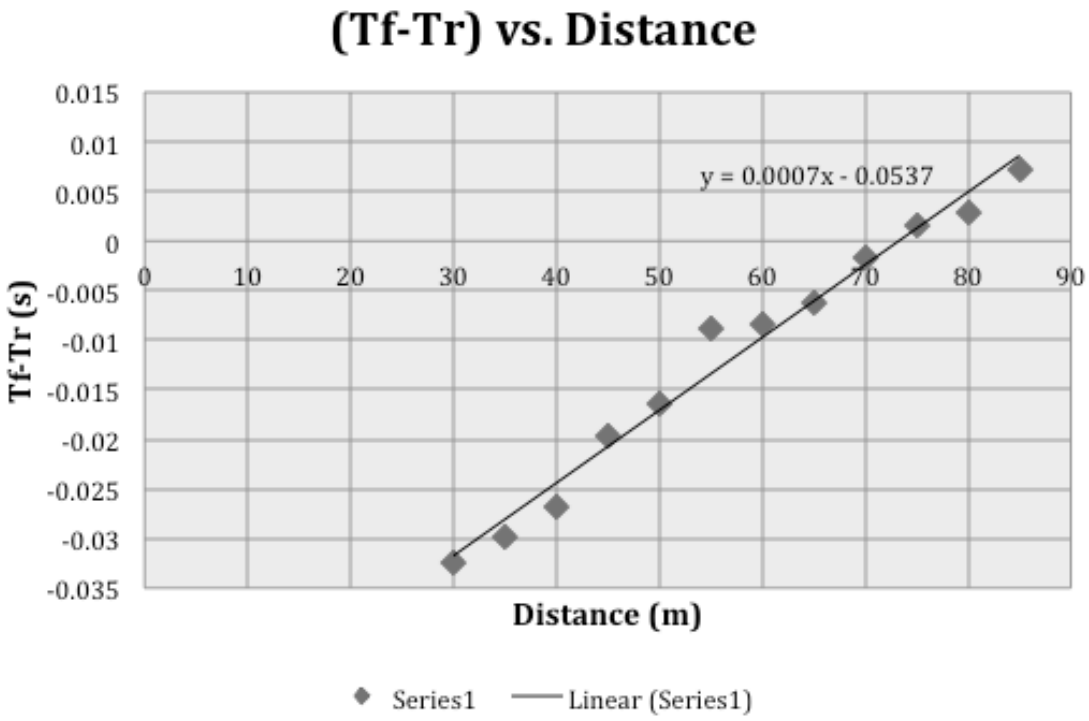

Figure 18. *The figure plots Tf-Tr for shots 4 and 5. The linear equation gives the slope of the best-fit line that can be used in Equation 3 to obtain a value for V_2.*

End to End Travel Time (s)
0.06535375

Figure 19*. Estimated value from the data that gives the end-to-end travel time. This value is used to calculate delay time.*

Tf+Tr (s)
0.0574807
0.0662044
0.0752707
0.0798392
0.0788322
0.0791878
0.0784268
0.081426
0.0825108
0.0838522
0.0834106
0.0848146
0.0874916
0.0859695
0.0864187
0.085388
0.085376
0.0872867
0.0899687
0.0918734
0.0923597
0.0921989
0.0910768
0.0938126

Figure 20. *Table displays calculated values for the plus terms in seconds.*

Similar to *Equation 3* above *Equation 5* was calculated for each receiver channel. ***Figure 20*** directly above shows these results.

$$T_f + T_r \qquad \textbf{Equation 5}$$

As the wave travels away from the source to the boundary of the bedrock the time by which it takes is referred to as the delay time ***(Figure 21)***. This delay time is calculated using *Equation 6*.

$$\frac{1}{2}\left[\left(T_f + T_r\right) - (End\ to\ End\ Travel\ Time)\right] \qquad \textbf{Equation 6}$$

Delay Times (s)
-0.003936525
0.000425325
0.004958475
0.007242725
0.006739225
0.006917025
0.006536525
0.008036125
0.008578525
0.009249225
0.009028425
0.009730425
0.011068925
0.010307875
0.010532475
0.010017125
0.010011125
0.010966475
0.012307475
0.013259825
0.013502975
0.013422575
0.012861525
0.014229425

Figure 21. *Table displays calculated values for delay times in seconds. The central bulk of the data is of most importance because it has the least amount of noise.*

Plotting the delay times against the distance from the forward shot can create a time depth plot (***Figure 22***).

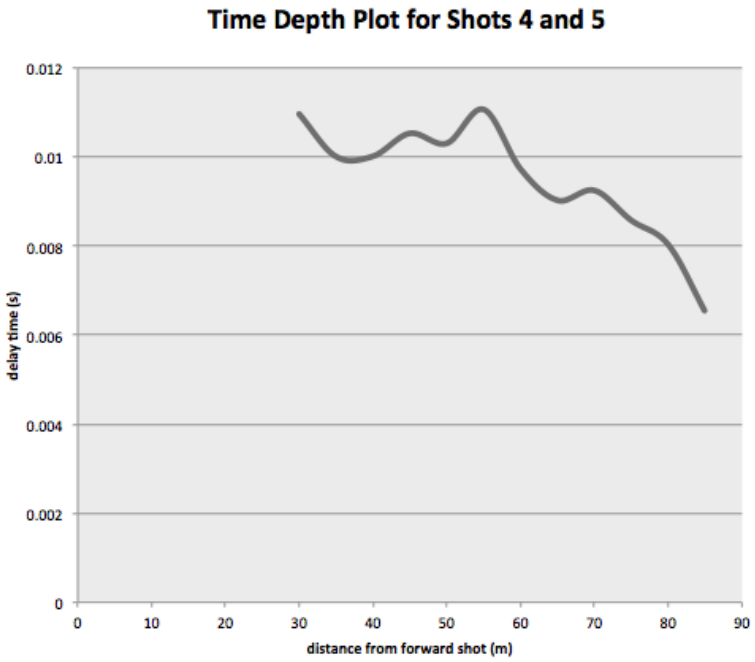

Figure 22*. Plot displayed above is a time to depth plot for shots 4 and 5. This figure is used as another tool to visualize the experimental data with depth. Delay time increases the further the receiver is from the source because the wave has a further distance to travel.*

Determining a value for V_1 was one of the more challenging parts. The way it is directed in the Plus-Minus method is to simply measure V_1 as the average measured from the direct wave for the forward and reverse shot. This method is displayed below in ***Figure 23***.

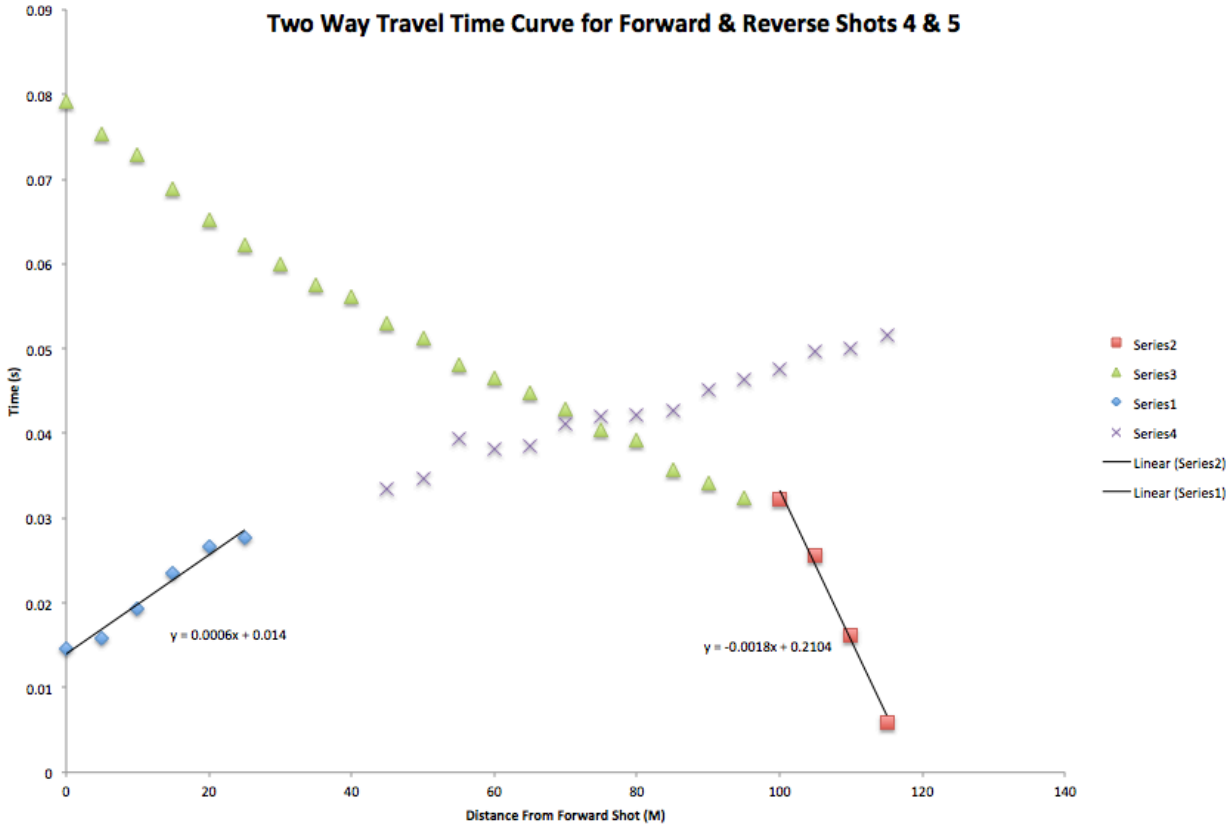

Figure 23. *Graphical display of the two way travel time curve for forward and reverse shots 4 and 5. This graph is used to obtain a value for V_1 using the steps in the Plus-Minus method. The best-fit lines are applied to the direct lines of both forward and reverse shots with corresponding linear equations. V_1 is the inverse of the slope.*

V1 is measured as the average measured from direct wave for forward and reverse shots. So that is just the average of the inverse slope obtained in ***Figure 23***.

$$\frac{1}{.0006} = 1666\ \frac{M}{s} \qquad \frac{1}{.0018} = 555\ \frac{M}{s}$$

$$\frac{(1666 + 555)}{2} = 1110\ \frac{M}{s} = V_1$$

V1 (M/s)	V2 (M/s)
1110	2857

Knowing V_1 and V_2 makes it possible to calculate the critical angle:

$$\arcsin\left(\frac{V_1}{V_2}\right) = 0.399 = \theta_c$$

The critical angle is used to calculate the depth to bedrock (***Equation 7***).

$$\frac{[(Delay\ time)\times(V_1)]}{\cos\theta_c} = Depth\ to\ Bedrock \qquad \textbf{\textit{Equation 7}}$$

Depth to Bedrock (m)
-4.74207786
0.512361605
5.973155134
8.724843832
8.118309845
8.332494042
7.874130224
9.680601658
10.33399597
11.14194501
10.87596149
11.72161563
13.33402028
12.41723241
12.68779355
12.06698463
12.05975682
13.21060537
14.82602161
15.97325625
16.26616338
16.16931068
15.49344992
17.14127085

The values in green are used because they are the closest to an average depth and they have the least amount of noise and outside interference within the experimental data.

Seismic Line	V1 (M/s)	V2 (M/s)
Seismic Line 1	1110	2857
Seismic Line 2	902	2222
Seismic Line 3	563	1666
Seismic Line 4	533	1666

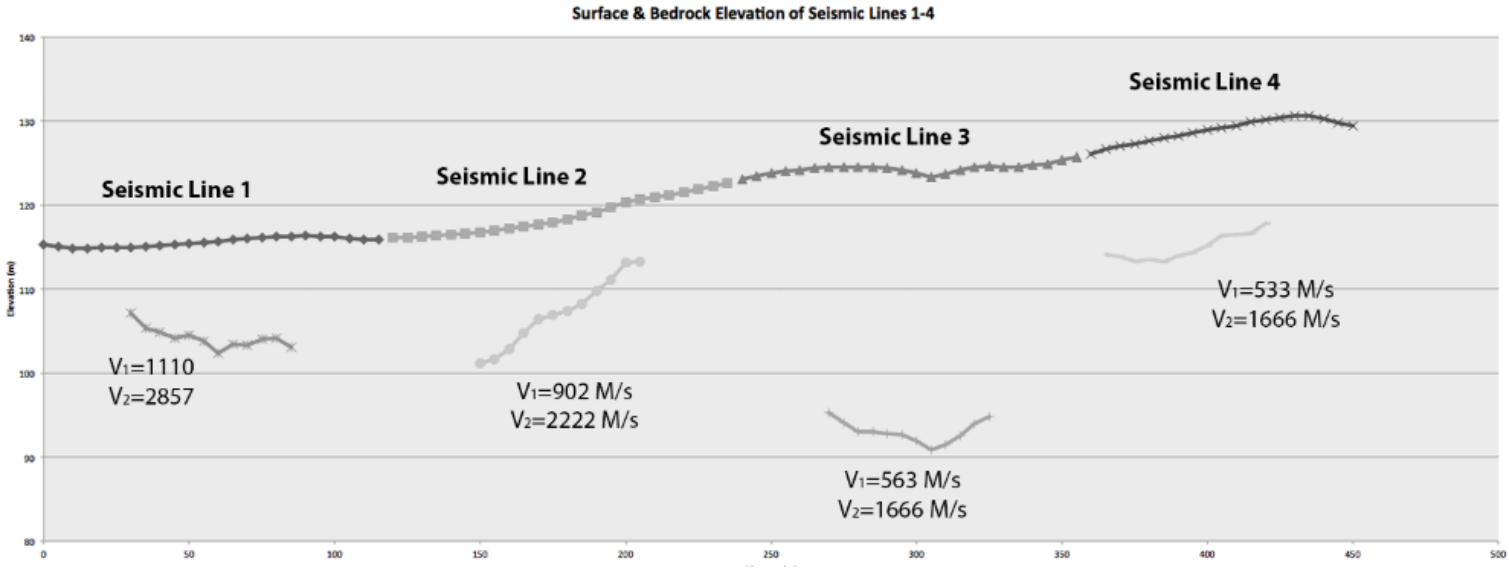

Figure 24*. This is a graph of the surface elevation with the calculated bedrock elevation for seismic lines 1-4. The velocity values used in the depth to bedrock calculations are given underneath each section of bedrock elevation. These values were calculated using the experimental data and strictly by following the summary of steps for the Plus-Minus Method.*

Figure 24 above is a visual representation of bedrock elevation calculated as the depth to bedrock values referenced to the surface elevation, which was obtained from the Leica RTK GPS data. The depth to bedrock was calculated by following the summary of steps for the Plus-Minus method. This method of calculating bedrock depth is as accurate of data as we could have gotten had we not collected seismic refraction data on the 23-meter lines. Fortunately we did, and the velocity values

obtained from these seismic lines can be assumed to be a good representation for V_1 of that general area.

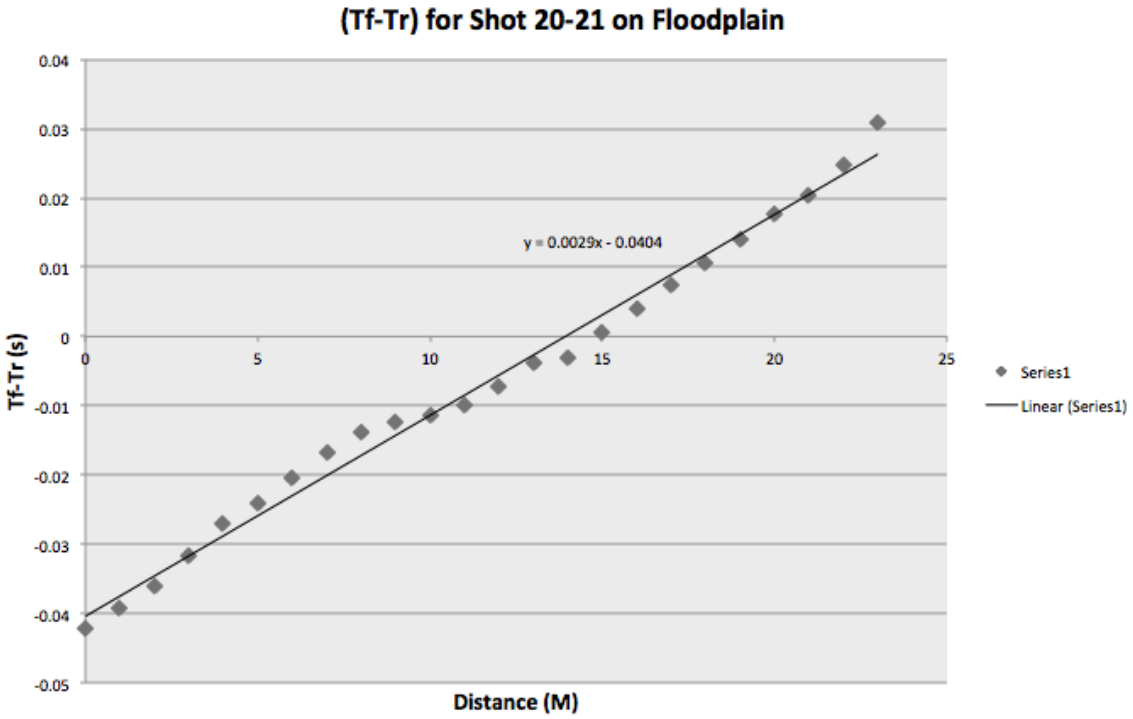

$$Velocity = \frac{2}{.0029} = 689\ (\frac{M}{s})$$

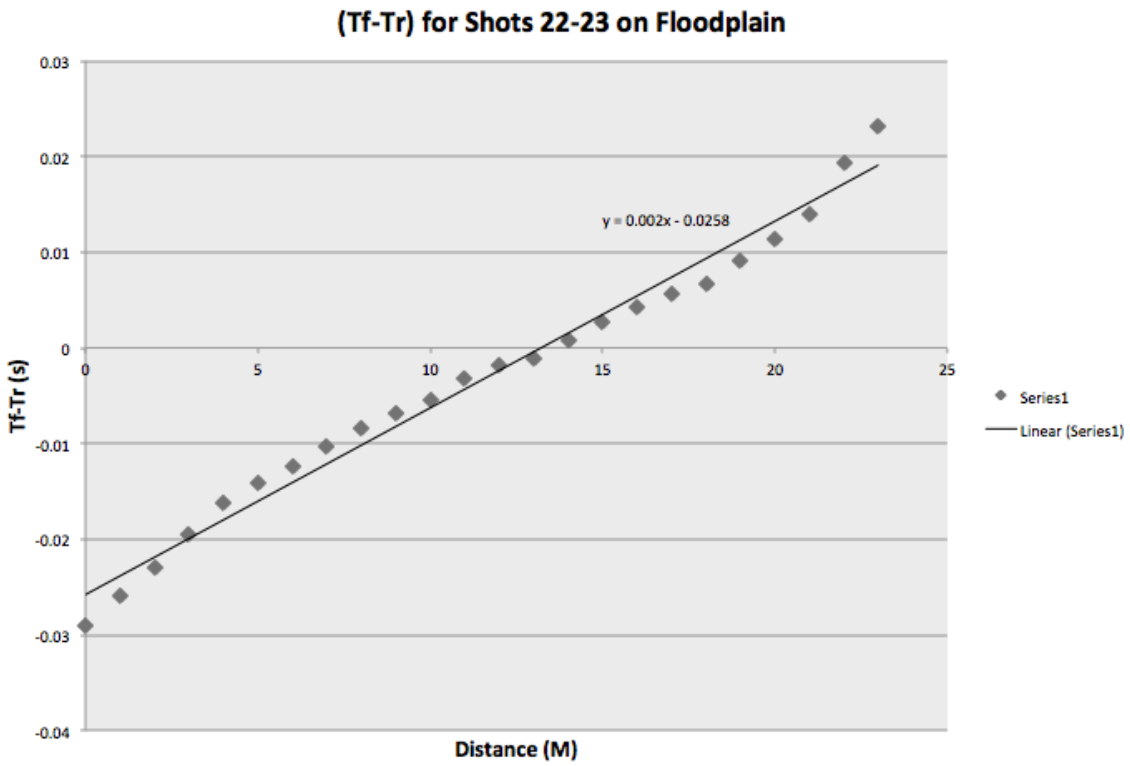

$$Velocity = \frac{2}{.002} = 1000\ (\frac{M}{s})$$

Figure 25. *The above plots displays the calculated minus terms from the experimental data for shots 20 and 21, as well as shots 22 and 23. A line of best fit was applied to the data and the linear equation to accompany it is given. Wave velocity is related to the slope given in the linear equation. The Velocity is calculated under each plot.*

Averaging these two velocities further constrains the most likely value for V_1 on the floodplain (***Figure 25***).

$$Average\ V_1 Value = \frac{689 + 1000}{2} = 845\ \frac{M}{s}$$

The same approach for constraining a value for V_1 was performed for the seismic lines on the terrace. Note however, that for Seismic Line 2 I used a value of

655 for V_1 that is the average of the floodplain and terrace. I chose to do this because while technically the geomorphic mapping group included it in the terrace area I felt it was more of a transitional zone.

Seismic Line	V1 (M/s)	V2 (M/s)
Seismic Line 1	845	2857
Seismic Line 2	655	2222
Seismic Line 3	465	1666
Seismic Line 4	465	1666

Using each of these velocities to get depth to bedrock values for the experimental data allowed me to create a graphical cross section of the main survey line (***Figure 26***). The new values provide a range of possible bedrock depth for each corresponding seismic line.

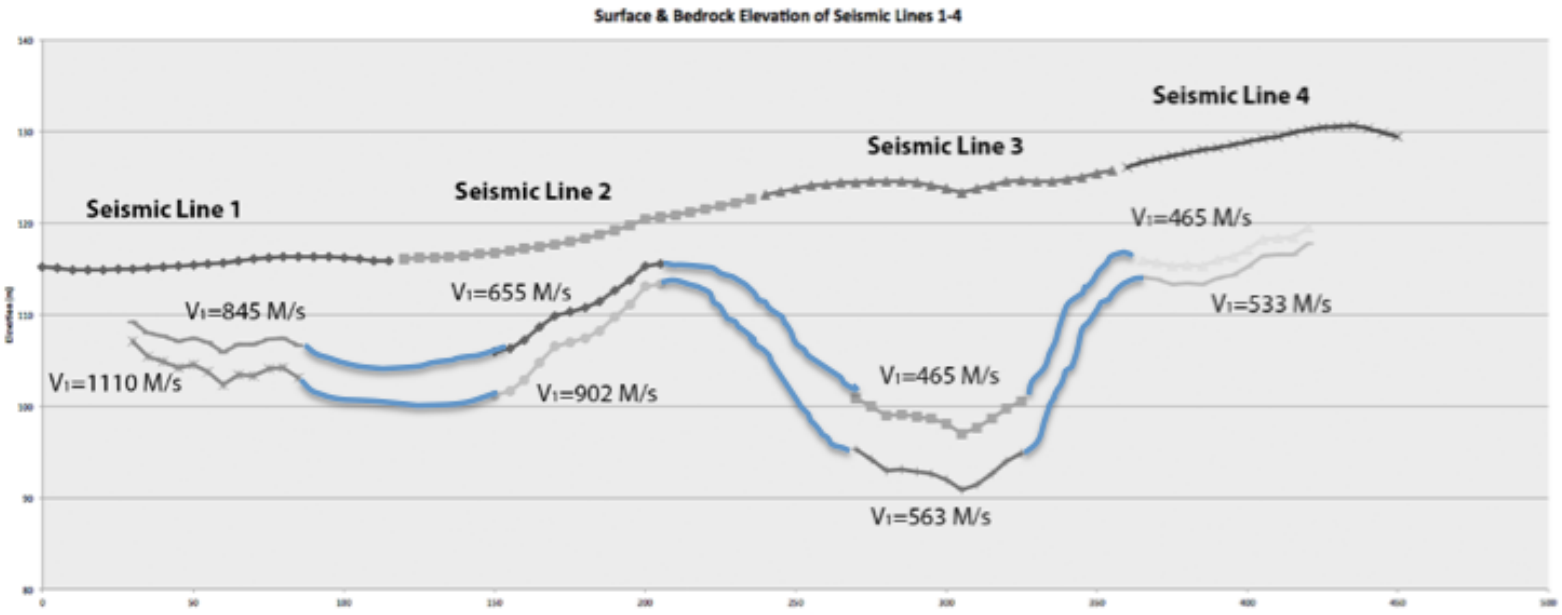

Figure 26. *This is a graph of the surface elevation with the calculated bedrock elevation for seismic lines 1-4. The velocities values used in the depth to bedrock calculations are given next to each section of bedrock elevation. These values have been constrained giving a range for bedrock to fall into. The lower bound values were calculated by following the summary of steps for the Plus-Minus Method. The upper bound values were calculated from the 25-meter seismic lines for both the flood plain and the terrace. The blue lines connecting the bedrock elevations are purely approximations.*

Seismic Line 3 had some of the worst experimental data, and as a result the bedrock elevation is anomalous compared to the surrounding elevations. In the field when data for Seismic Line 3 was being collected there was a lot of background noise. Miscommunication between seismic refraction group and the sediment cores group occurred when the coring members continued to drill core while seismic refraction data was being collected. Unfortunately they were in close proximity, so the energy dissipated from their machines interfered with the energy source. Also, Aslan was not able to hit the metal plate in the center consistently, which led to further poor data on Seismic Line 3.

Seismic Line 5 was off the path of the main survey line (Seismic Lines 1-4) and on the terrace. The velocity values were calculated in the same way as they were for the lower bound values on the main survey line. V_2 was obtained by plotting the minus values and fitting a line of best fit to the central values and then using the slope from that linear equation. V_1 was calculated from the 23-meter line that was at the base of Seismic Line 5.

Seismic Line	V1 (M/s)	V2 (M/s)
Seismic Line 5	465	2222

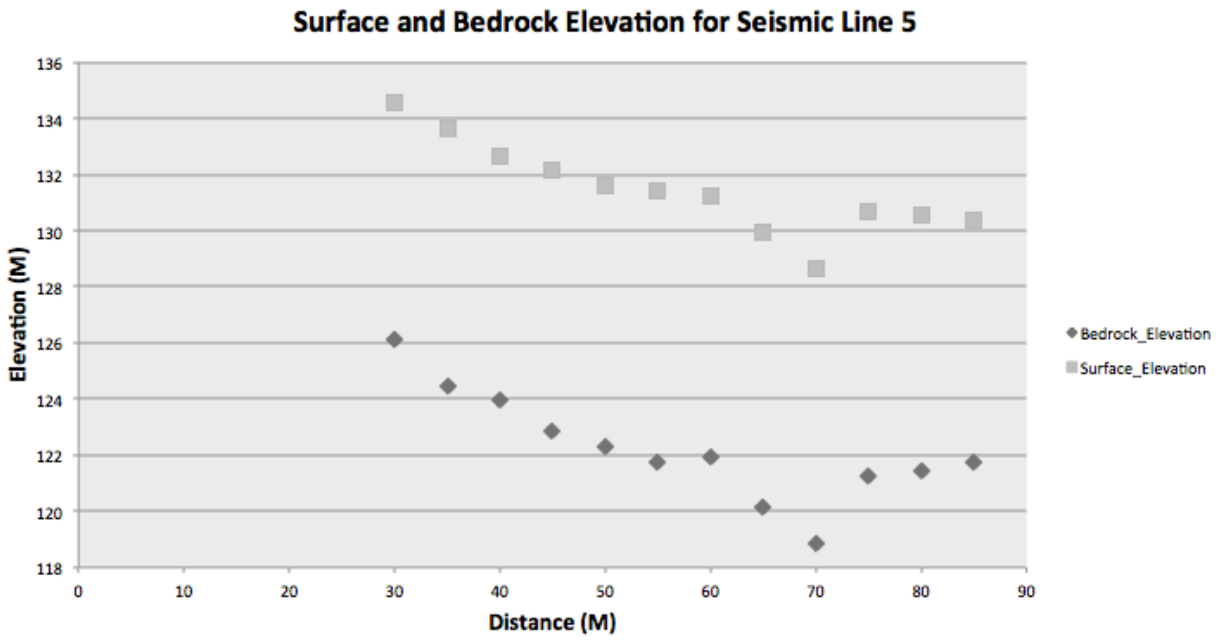

Figure 27. *The figure is a graphical representation of the surface and bedrock elevation for Seismic Line 5. On average the bedrock is about nine meters below the surface.*

Seismic Line 5 shows about an on average depth between the surface and bedrock of about nine meters (***Figure 27***). In the field we hypothesized that the bedrock would be significantly closer to the surface if not only a meter or two down. If time allowed a sloped method could be applied to the experimental data to check for a shallower bedrock depth.

Seismic Line 6 was the last data collected for the 115-meter lines and ran perpendicular to the river and parallel to Seismic Line 1. The velocity values were calculated in the same way as they were for the lower bound values on the main survey line. V2 was obtained by plotting the minus values and fitting a line of best

fit to the central values and then using the slope from that linear equation. V1 was calculated from the two 23-meter lines that were positioned on either end of Seismic Line 6.

Seismic Line	V1 (M/s)	V2 (M/s)
Seismic Line 6	845	2222

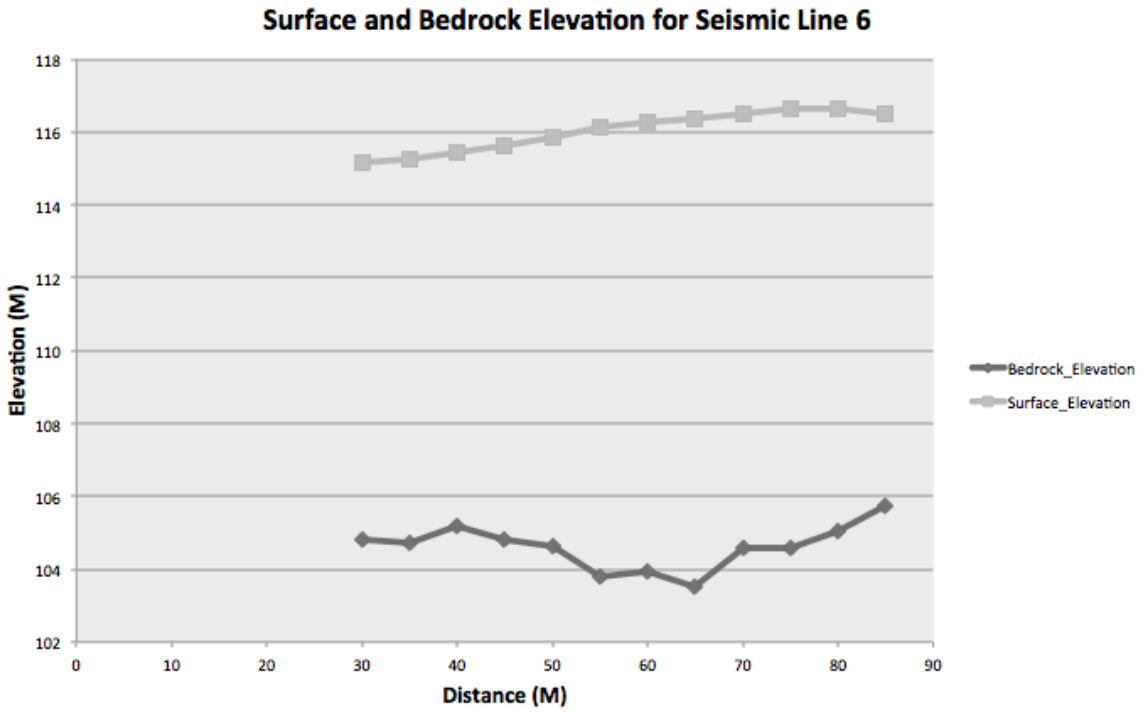

Figure 28*. The figure is a graphical representation of the surface and bedrock elevation for Seismic Line 6 on the floodplain. On average the bedrock is about eleven meters below the surface.*

Seismic Line 6 shows about an average depth between the surface and the bedrock of about eleven meters. In the field we hypothesized that the bedrock was around 10 meters below the surface. ***Figure 28*** shows that our hypothesis was probably correct.

b. Electrical resistivity:

During the first day of field work the members of the electrical resistivity set up and collected data from five electrical resistivity lines: R100-156, R200-256, R300-356, R401-457, and R500-556 (***Figure 29***). Each of the five transects consisted of a cable that had 54 electrodes spaced at two meters and a single SuperSting with Wi-Fi instrument that was connected to a 12 Volt battery.

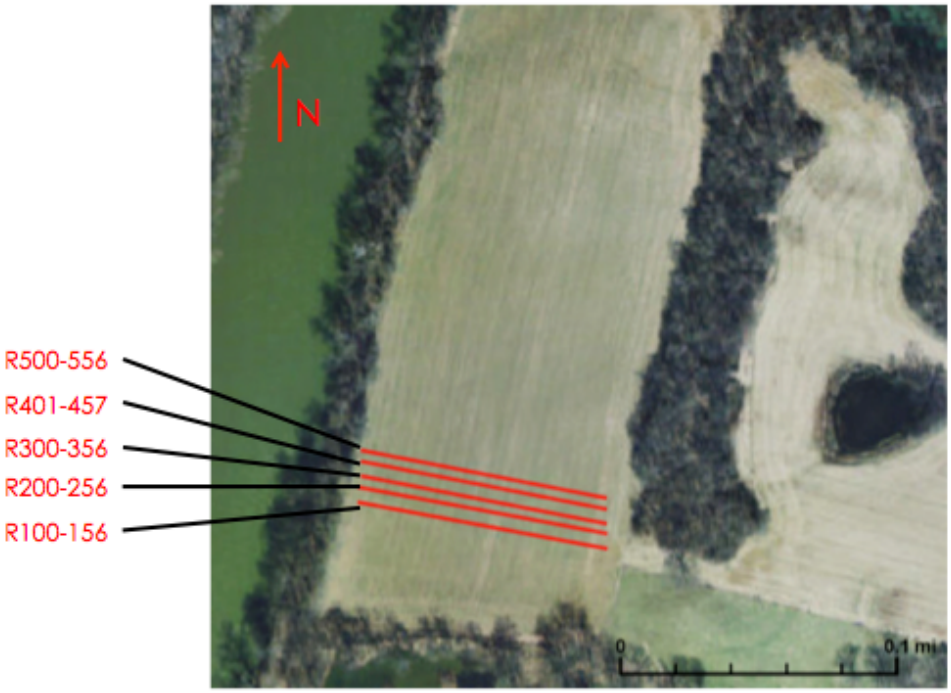

Figure 29. *The figure is an aerial view showing the approximate locations of the five electrical resistivity survey lines. The surveys were conducted from South to North. Note that GPS data was not collected for the electrical resistivity survey lines. (Fenerty & Baer, 2013)*

The electrical resistivity raw data was not made public. Jason from Advanced Geosciences Inc. provided the equipment for the study. Because they own the rights to the software that is used to reduce the data Jason reduced the data himself and

provided us with the best-fit images that plotted the apparent resistivity with depth for each of the five electrical resistivity lines seen below in ***Figure 30***.

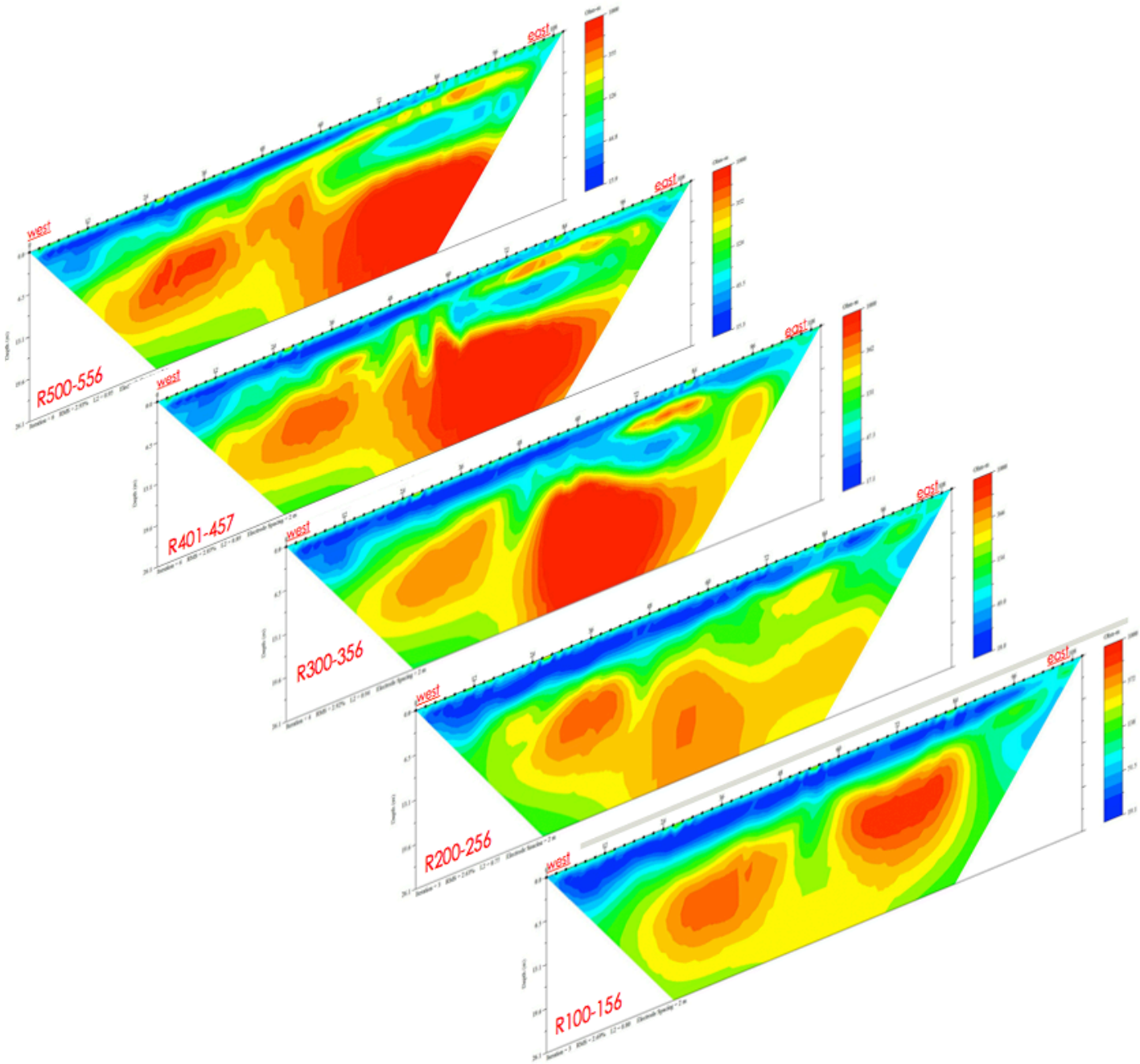

Figure 30. *Figure shows experimental data for electrical resistivity surveys imaged and contoured as apparent resistivity plotted at depth. The software used was EarthImager 2D. Survey lines R100-156, R200-256, R300-356, R401-457 and R500-556 are plotted next to each other at a 22.5-degree angle to provide depth. Blue represents materials with relatively low resistance, and red represents materials that*

are the most resistant. Note that the accuracy of the data decreases from the top most central location moving outwards.

The results of the data analysis show that the depth to bedrock is around 10-meters. There is also an erosional feature because on the east side of the figure there is less resistant material underneath higher resistant material. Erosional processes removing material and having less resistant material deposit over time and then have more resistant material erode over top that less resistant material could cause this. Southern Indiana, and this field study area in particular contain karst topography (***Figure 31***). The Geomorphology group pointed out that the pond present on the terrace could be a sinkhole that could be a modern analogy for this particular anomaly.

Figure 31. *Figure depicts an aerial view of recorded sinkholes as of 2011 in the surrounding area. (Fenerty & Baer, 2013)*

c. Ground Penetrating Radar (GPR):

The ground penetrating radar (GPR) group collected data from 31 separate lines. Of these lines 29 is of the most importance (***Figure 32***).

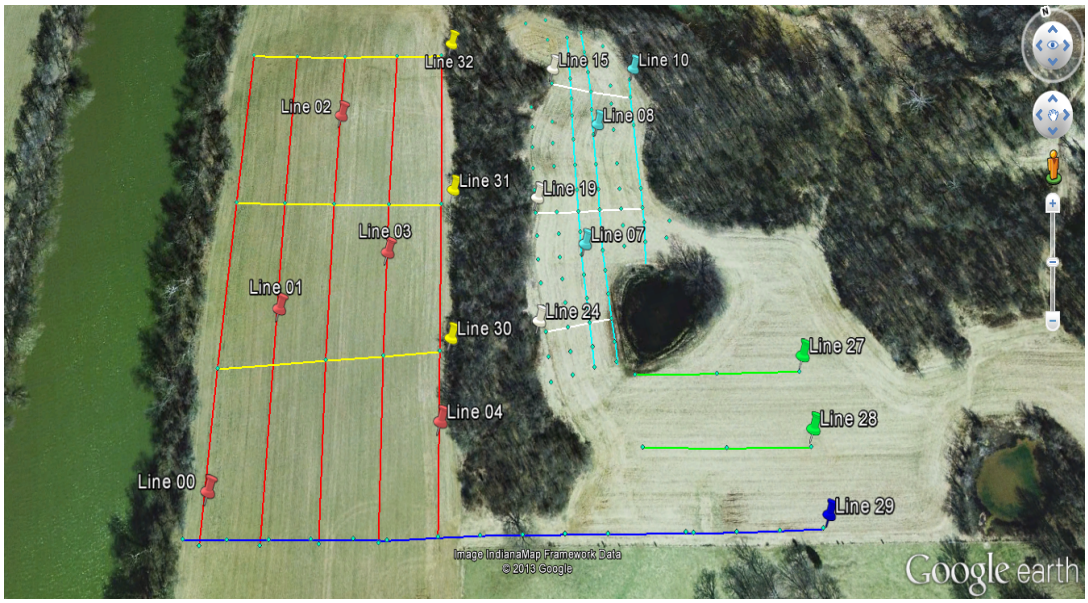

Figure 32. *Aerial view of the 31 lines that the ground penetrating radar (GPR) group collected data from. Data collected from the blue transect is important because it can be compared to other geophysical and core data collected. Note that GPS locations were collected along each line. (Figure taken from GPR PowerPoint presentation)*

The software used to reduce the data was called Win EKKO Pro v1.0. The software would take the collected data and average the refracted radio frequencies creating a spectrum plot of the average amplitude. The raw data was then processed through a sequence of steps to produce a relatively accurate visual cross section of the near surface stratigraphy (***Figure 33***).

The sequence of data reducing steps is described below:

1. Dewow Processing:
    - Removes unwanted low frequencies caused by electrical properties of the ground, all the while preserving the high frequency signal.

2. Low Pass Filter (LPF):
    - Filters out frequencies above a certain cutoff frequency using a recursive algorithm.
3. Migration:
    - Measures diffraction hyperbole by focusing scattered signals and collapsing the hyperbolic responses to point targets.
4. Automatic Gain Control (AGC):
    - Attempts to equalize all signals by applying a gain that is inversely proportional to the signal strength.

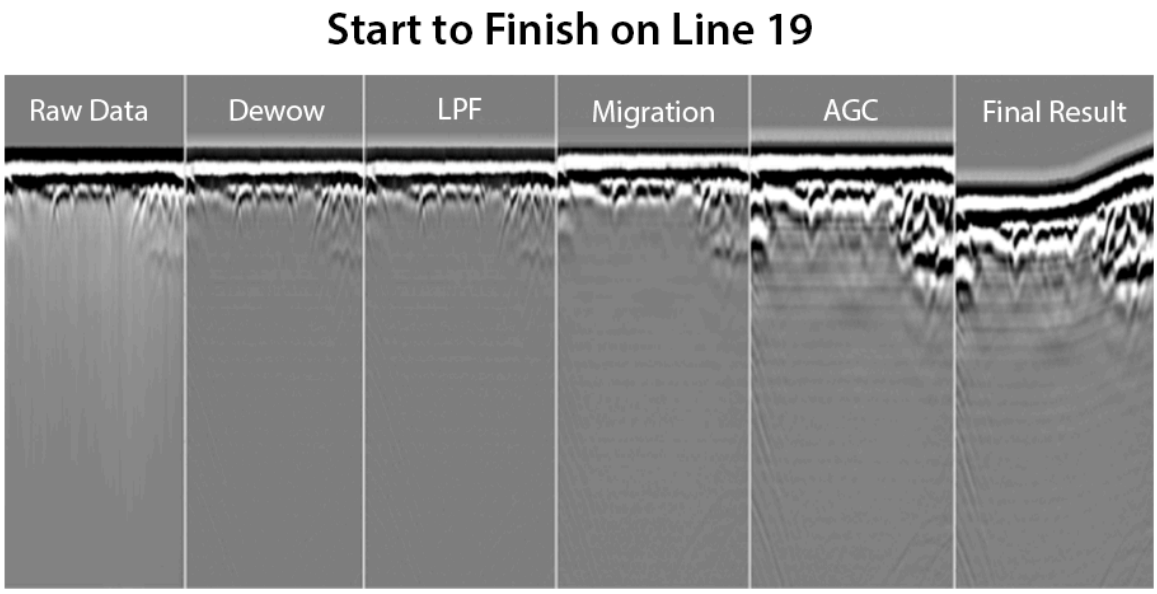

Figure 33*. Start to finish of the sequence of steps taken to reduce the GPR data for Line 19. (Modified figure from the GPR PowerPoint presentation, 2013)*

As stated before the most important data acquired from the GPR group is that from Line 29 (***Figure 34*** & ***35***). Line 29 runs perpendicular from the river starting on the floodplain running to the top of the terrace. This line runs parallel to the main seismic refraction survey line (Seismic Lines 1-4).

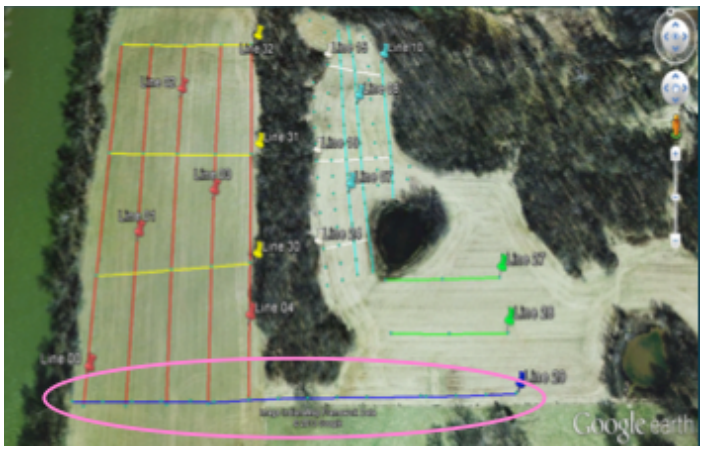

Figure 34*. Aerial view of the 31 GPR lines with line 29 circled in pink. (Figure acquired from the GPR PowerPoint presentation, 2013)*

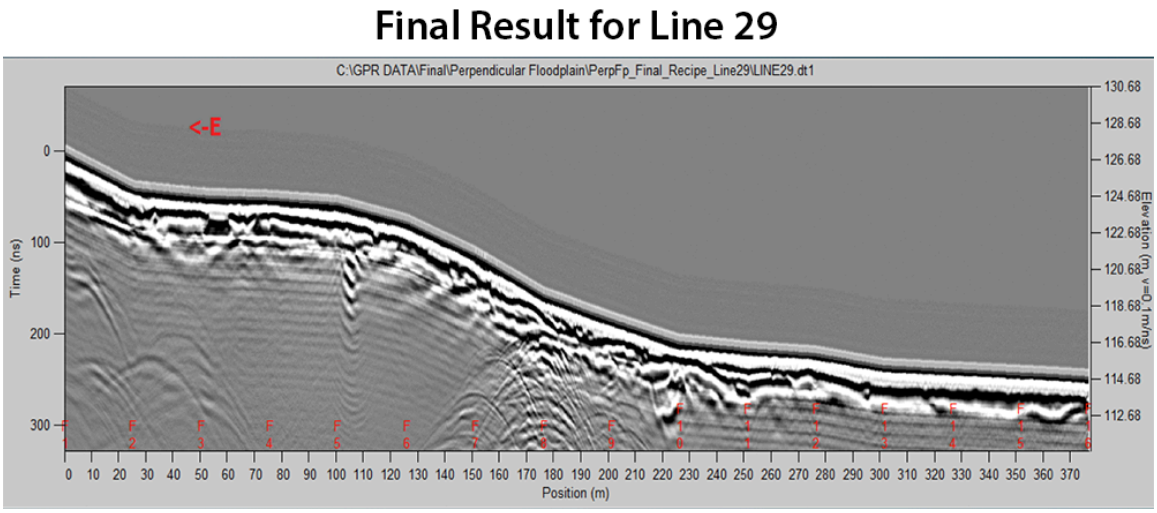

Figure 35*. Final result of experimental GPR data acquired along Line 29. (Figure from GPR PowerPoint presentation, 2013)*

Common errors involved in GPR data consists mainly of scattered signals caused by man-made structures such as fences, geologic layers that do not reflect such as clay, and anomalous material such as boulders.

d. Core:

The sedimentary core group extracted and analyzed nine sediment cores that ranged from sixteen to twenty four feet in length. The locations of the extracted cores can be seen in ***Figure 36*** below.

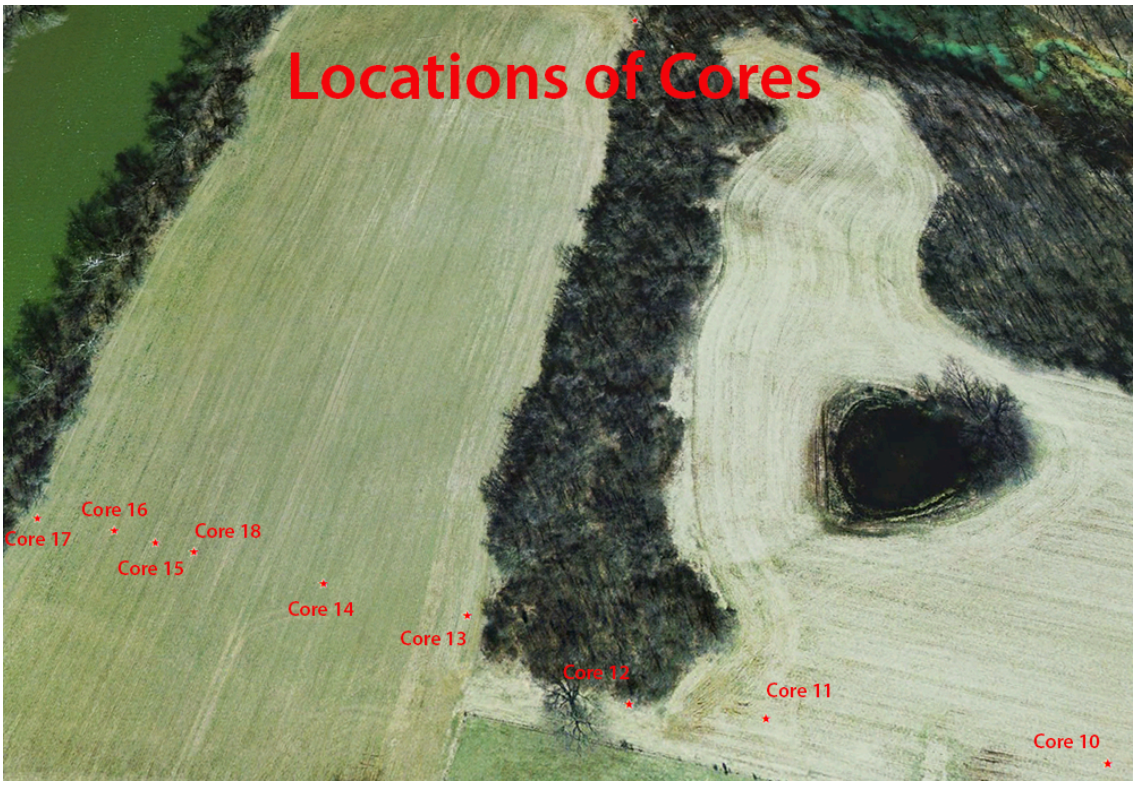

Figure 36*. Locations of all nine well holes. The wells correlate to the main seismic refraction survey (Seismic Lines 1-4), as well as with Line 29 from the GPR data. (Modified from Core presentation, 2013)*

Members of the sedimentary core team analyzed every ten centimeters of the core to create stratigraphic logs for the nine wells drilled (***Figure 37***).

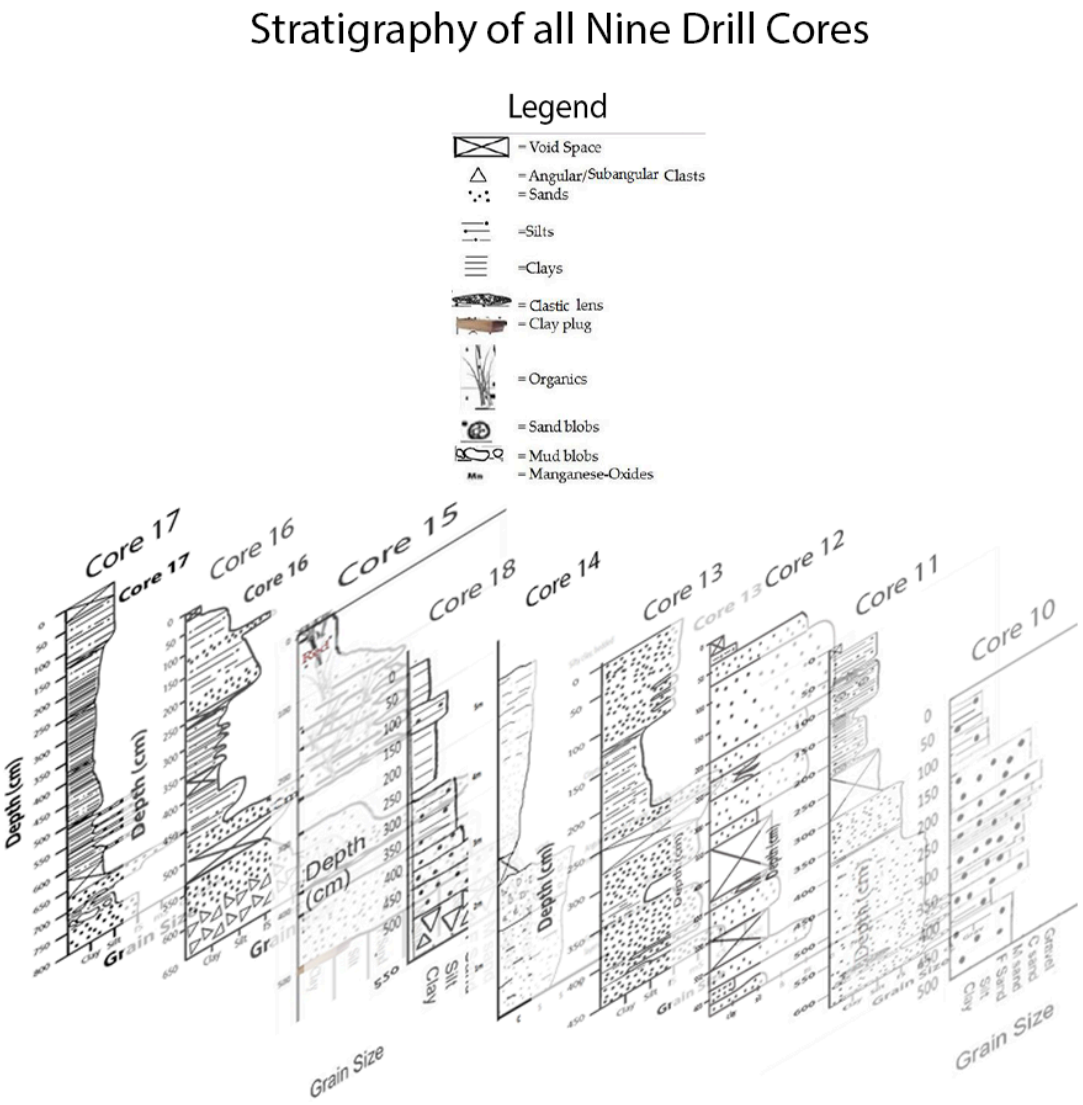

Figure 37*. Figure depicts the stratigraphy of all nine-drill cores in locational order. (Modified from Core presentation)*

Interpretation

The field study area is located along the banks of the white river, which is actively controlling the geology of the study area. The river is constantly eroding away the banks of the levee, the thalwag of the river is probably carving into the underlying limestone bedrock and when it floods onto the floodplain it deposits a layer of alluvium.

The formation of the white river begins during the last ice age, which occurred during the Pleistocene or roughly 3-million years ago. During this time the entirety of North America was covered in glaciers, which ebbed and flowed across the land. The glaciers gave rise to the present day sediments we find in Northern Indiana in the form of till deposits (Thornbury 1940). This till was washout from the glaciers (the Illinoian & Wisconsin) that covered Northern Indiana during the Pleistocene. The Illinoian glacier retreated from Northern Indiana around 45,000 years ago, and the glacial run off led to the formation of the White River basin, along with the field study area (Thronbury 1950).

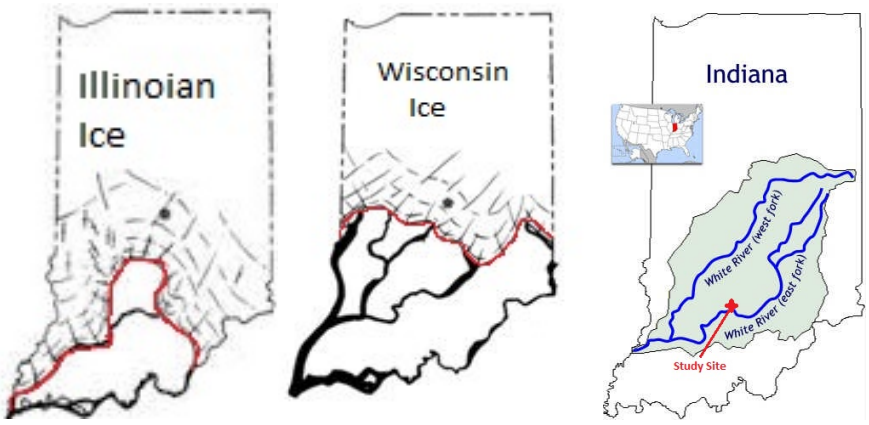

Figure 38. *Estimated locations of Pleistocene glaciation in Indiana to scale with the White River basin and our field study area. (1)*

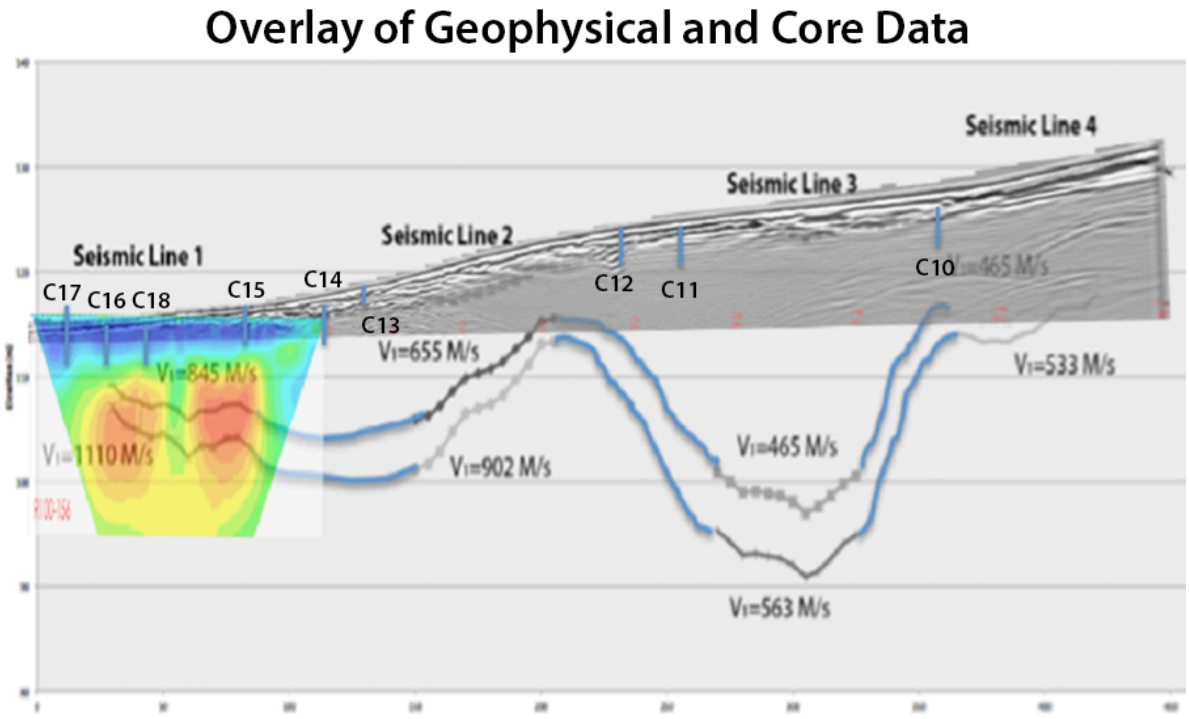

Figure 39. *Very crude approximation of all geophysical and core data along the original seismic refraction survey line (Seismic Lines 1-4).*

The best data collected from the field study area was on the floodplain. This is simply because all three types of geophysical data (seismic refraction, electrical resistivity, and GPR), and drill cores were taken here. ***Figure 39*** roughly shows reduced data from each of the geophysical methods overlaid on top of one another with approximate locations of drill cores.

Depth to bedrock for seismic data was approximated at around nine to ten meters below the surface for Seismic Line 1. Core 16 was six and a half meters deep and contained gravel derived sediments. Core 18 contained similar gravel materials and was around six meters deep. However, Core 17 was eight meters deep and contained no material of gravel size.

The Electrical resistivity showed anomalous areas of interest beginning at around ten meters below the surface. This is represented in red in ***Figure 39.*** The anomalies lie just below the drill cores and just within the seismic refraction bedrock range.

The electrical resistivity data shows signs of erosional or solution collapse features which are most likely occurring in karst. Referring back to ***Figure 30*** there is a clear path of separation between the anomalous zones that could have been a meandering stream from the receding glaciers or an ancient river channel long evolved.

In conclusion the formation of the field study area began roughly 60,000 years ago with the receding of the North American glaciers and the huge influx of water that brought meandering streams and glacial till to Southern Indiana. The stratigraphy includes alluvium sediments from the river, glacial till, a mix of alternating sandy silty layers with a gravel layer stratigraphically above the limestone bedrock. The best estimate for depth to bedrock on the floodplain is between nine to eleven meters.

References

1. "Geologic and Cliamtologic Setting." *Central Indiana Water Resource Partnership*. N.p., n.d. Web. 17 Dec. 2013.

2. "Google Images." *Google Images*. N.p., n.d. Web. 17 Dec. 2013.

3. "Seismic Refraction Method." *Sesimic Refraction Method*. N.p., n.d. Web. 17 Dec. 2013.

4. "Snell's Law." *Wikipedia*. Wikimedia Foundation, 12 July 2013. Web. 17 Dec. 2013.

5. Thornbury, William D. *Glacial Sluiceway's and Lacustrine Plains of Southern Indiana*. State of Indiana, n.d. Web.

6. Thornbury, William D. “Weathered Zones and Glacial Chronology in Southern Indiana”. The Journal of Geology. 48. 5. (1940): 449-475. Web.

7. United States of America. Department of Conservation. *Glacial Sluiceway's and Lacustrine Plains of Southern Indiana*. By William D. Thornbury. Bloomington: State of Indiana, 1950. Print.